

Preparation and characterization of biopolymer electrolyte based on cellulose acetate for potential applications in energy storage devices

S. Monisha^{1,2} · S. Selvasekarapandian² · T. Mathavan¹ · A. Milton Franklin Benial¹ · Sindhuja Manoharan² · S. Karthikeyan³

Received: 13 February 2016 / Accepted: 9 May 2016 / Published online: 18 May 2016
© Springer Science+Business Media New York 2016

Abstract In this present work, the solution casting technique was utilized to develop the proton conducting solid biopolymer electrolyte by the complex formation of cellulose acetate (CA) with the ammonium thiocyanate (NH_4SCN) salt. The crystalline nature and complex formation of CA with different concentrations of NH_4SCN were investigated using X-ray diffraction (XRD) and Fourier transform infrared (FTIR) spectroscopic techniques. The XRD analysis revealed that the amorphous natures of the CA complex were increased with increase of NH_4SCN salt concentration, which leads to the higher ionic conductivity. The FTIR analysis confirmed the complex formation between CA and salt matrix. Differential scanning calorimetry (DSC) was used to predict the glass transition temperature (T_g) values, which reveals that the T_g value increase with respect to the increase of NH_4SCN concentration. The electrical conductivity was measured using AC impedance analyzer, which showed that the magnitude of ionic conductivity increases with an increase in salt concentration up to 50CA:50 NH_4SCN . The 50CA:50 NH_4SCN has maximum ionic conductivity value of $3.31 \times 10^{-3} \text{ S cm}^{-1}$. Transference number measurement was carried out to investigate the nature of the charge transport species in the polymer electrolyte. The proton battery was constructed with the highest conducting

polymer electrolyte 50CA:50 NH_4SCN and its open circuit voltage with load were studied. Hence, the present investigation paves the way for the development of fuel cell and primary proton battery applications.

1 Introduction

In green economy, the demands for biopower enhance the technological interest in the field of solid polymer electrolyte (SPE). In recent years, this highly specialized field encompasses to play a vital role in designing energy based devices, replacing liquid electrolyte in fuel cells, electrochemical sensors, batteries and electro chromic devices [1, 2]. The SPE provides good contact surface with electrodes, good shelf life, less problem with leakage or pressure distortion and also the SPE is easy to prepare and very affordable [3, 4]. However, the synthetic polymer in SPE faces disadvantage and not being environmentally green. Hence, it is imperative to develop the biopolymer electrolytes by using natural polymer, which has gained more and more attention, owing to their abundant in nature, low cost, friendliness to the environment and potential as substitute for some petrochemicals [5]. In this way, an ideal solid biopolymer (SBP) in the polymer electrolyte system contributes to free pollution and it has directly brought forward green nation, which fosters the interest in research to address the environmental crises. Chitosan, starch, pectin, methyl cellulose and cellulose acetate are natural polymers, which have been proposed by researchers to develop SBP electrolytes [3, 6, 7]. Among these natural polymers, cellulose acetate (CA) is an important natural polymer, which is the acetate ester of cellulose and very attractive for its abundance in nature, low cost, film forming nature and easy disposal [8]. The CA has polar groups that possess lone pair electrons, which facilitates the

✉ S. Selvasekarapandian
sekarapandian@rediffmail.com

¹ Research Department of Physics, N.M.S.S. Vellaichamy Nadar College, Madurai, Tamilnadu 625 019, India

² Materials Research Center, Coimbatore, Tamilnadu 641 045, India

³ Department of Physics, Madras Christian College, Chennai, Tamilnadu 600 059, India

ionic conduction. However, the high glass transition temperature, rigidity or high crystalline nature of CA hindered its applications [9, 10], which can be overcome by adding inorganic salts to the CA. The gel polymer electrolyte CA has been used as a separator for various kinds of batteries, such as lead acid batteries and silver-zinc rechargeable batteries.

Johari et al. [11, 12] studied the composite of CA based gel polymer electrolyte for proton batteries and reported the ionic conductivity, which was found to be (10^{-2} S cm^{-1}) and compared to solid polymer electrolyte. Although, its poor mechanical property, high evaporation and easy leakage stalled its electrochemical application [13]. Abidin et al. [14] carried out an electrochemical study on CA-Lithium bis(oxalato)borate (LiBOB) gel polymer electrolyte. The biodegradable polymer CA doped lithium perchlorate (LiClO_4) has been studied for supercapacitors by Selvakumar et al. [15]. Performance of CA membrane with lithium salts especially for lithium polymer cells have been studied by Ramesh et al. [9, 10]. However, until today not much effort has been taken by researchers to develop CA as a solid membrane with proton salts. Ammonium salts are considered to be a good proton donor [16, 17]. The protonic transport in this polymer membrane generally involves motion of H^+ ion i.e., in addition to motion of proton ion the conductivity has also been associated with the segmental motion of the polymer chain [18]. Hashmi et al. [19] reported that the charge carriers in the poly(ethylene oxide) (PEO)-ammonium perchlorate (NH_4ClO_4) are H^+ ion and the conduction occurs through the exchange of ions between complexed sites. Preparation of biopolymer based chitosan with ammonium thiocyanate (NH_4SCN) has attracted many researchers for the development of high conducting biopolymer electrolyte [20, 21].

The present work aims to develop a novel proton conducting bio polymer electrolyte with CA as a host polymer while ammonium thiocyanate (NH_4SCN) were chosen as the ionic dopant. The prepared SBP electrolytes were characterized by Fourier transform infrared (FTIR), X-ray diffraction (XRD), electrical impedance spectroscopy (EIS) and transference number measurement (TNM). Moreover using these complex polymer electrolyte CA: NH_4SCN with high ionic conductivity, proton battery was constructed and its discharge characteristics were evaluated. Finally, the developed SBP electrolyte meets the goals of green environment and provides greater opportunity for future fuel cells and proton batteries.

2 Experimental

In the present study, polymer CA (Sigma Aldrich, product code 1001345520), and salt NH_4SCN were used as the raw materials. Dimethyl formamide was used as a solvent. The

polymer complex CA: NH_4SCN with different molecular weight percentages of 90:10, 80:20, 70:30, 60:40, 50:50 and 40:60 were stirred continuously for several hours until a homogenous mixture was obtained. The obtained solutions were poured into petri dishes and dried in oven at 60°C to ensure removal of the solvent traces. After drying the transparent, flexible films of thickness ranging from 0.22 to $0.16\ \mu\text{m}$ were obtained. XRD patterns were recorded at room temperature with X'pert pro diffractometer system using the $\text{Cu-K}\alpha$ radiation in the range of $2\theta = 10^\circ\text{--}60^\circ$. FTIR spectroscopy studies were carried out using BRUCKER spectrophotometer in the range $2300\text{--}600\ \text{cm}^{-1}$. DSC measurements were recorded using DSC Q20 V24.10 Build 122, TA instruments. Conductivity studies of polymer electrolytes were measured using HIOKI 3532 LCR meter in the frequency range from 42 to 1 MHz by sandwiching them using aluminum as the blocking electrodes.

3 Results and discussion

3.1 X-ray diffraction analysis

XRD measurements were performed for polymer electrolytes CA with different NH_4SCN concentrations to infer the degree of amorphocity at room temperature. Figure 1a–g shows the XRD patterns of pure CA and six CA doped with different concentrations of NH_4SCN . The XRD patterns indicate that the solid polymeric films were composed of a combination of crystalline and amorphous phases,

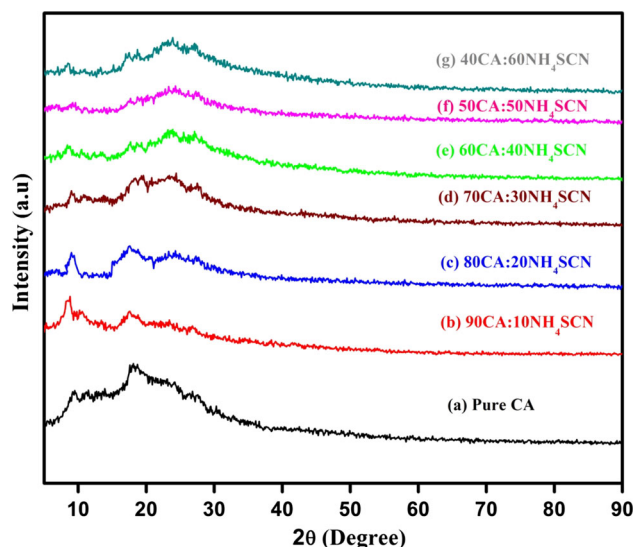


Fig. 1 XRD pattern for *a* pure CA, *b* 90CA:10 NH_4SCN , *c* 80CA:20 NH_4SCN , *d* 70 CA:30 NH_4SCN , *e* 60CA:40 NH_4SCN , *f* 50CA:50 NH_4SCN and *g* 40CA:60 NH_4SCN

which make the polymeric films to be in semicrystalline nature. The Fig. 1a indicates that the undoped polymer CA shows crystalline peaks at $2\theta = 9^\circ, 13^\circ, 18^\circ, 23^\circ$ and 27° , which correlates with the literature [9, 10]. The XRD patterns also indicates that the broadness of peak increases and its relative intensity decreases with increase of NH_4SCN concentration, which reveals that as ion concentration in the electrolyte increases, both the fraction of amorphous phase and charge carriers increases simultaneously [22]. From Fig. 1f, it was noted that 50CA:50 NH_4SCN has maximum amorphous nature. The increase in the amorphous nature causes a reduction in the energy barrier to the segmental motion of the polymer electrolyte resulting in high ionic conductivity [23]. This was interpreted in terms of Hodge et al. [24] criterion, which establishes a correlation between the intensity of the peak and the degree of crystallinity. On further addition of NH_4SCN concentration, the intensity of peaks increases for 40CA:60 NH_4SCN , which indicates the increase in crystallinity. This is because the polymer host was unable to accommodate the salt, which leads to the recombination of the ions [25]. The XRD patterns confirm the absence of peaks corresponding to pure NH_4SCN in the polymer electrolyte, which indicate the complete dissociation of the salt in polymer matrix.

3.2 FTIR analysis

In the present investigation, the FTIR spectroscopy was used to probe the complex formation and interactions between the polymer CA and salt NH_4SCN by means of change in the vibrational modes of polymer electrolyte under investigation. Figure 2 shows the FTIR spectra of pure CA and five CA doped with different concentrations of NH_4SCN and the corresponding vibrational frequencies were assigned and listed in Table 1.

The peak observed at 1736 cm^{-1} was assigned to C=O symmetric stretching in the aldehyde carbonyl group of CA [26]. The broad peak observed at 1436 cm^{-1} of pure CA was assigned to CH_3 bending. The absorption peak at 1371 cm^{-1} was attributed to CH bending of pure CA. The C–O stretching was observed at 1219 cm^{-1} for pure CA. The peak observed at 1030 cm^{-1} for pure CA was assigned to C–O–C Stretching of pyrose ring. The medium intensity peak observed at 901 cm^{-1} corresponding to pure CA was assigned to CH_2 rocking of vibrational mode. The observed peaks position and the intensity in FTIR ($1736, 1436, 1371, 1219, 1030$ and 901 cm^{-1}) were shifted due to the addition of 10, 20, 30, 40, 50 mol% of NH_4SCN with CA. The peak observed at 2055 cm^{-1} assigned to C \equiv N stretching, which was absent in pure CA. The intensity of peak observed at 2055 cm^{-1} was increased on addition of 10–50 mol% NH_4SCN with CA and it become sharp [27]. According to the literature, the observed peak at 2055 cm^{-1} is consistent

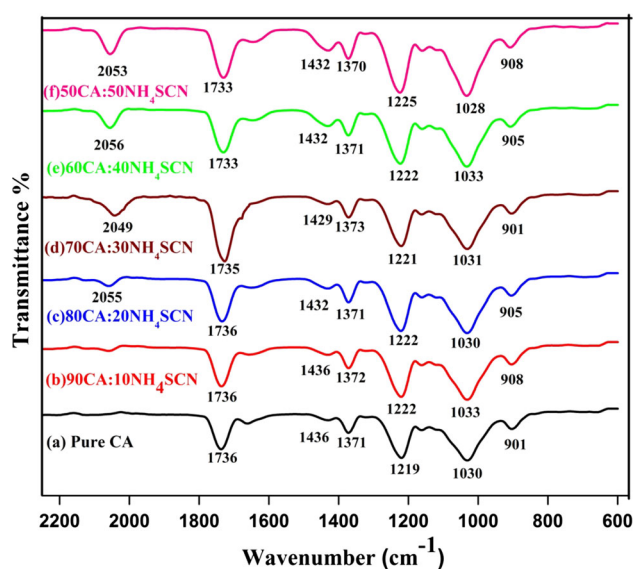


Fig. 2 FTIR spectrum for *a* pure CA, *b* 90CA:10 NH_4SCN , *c* 80CA:20 NH_4SCN , *d* 70 CA:30 NH_4SCN , *e* 60CA:40 NH_4SCN , and *f* 50CA:50 NH_4SCN

with the assignment of spectroscopically free SCN^- anion [28]. The formation of nitrogen or sulfur bonding give rise to spectral changes since the C \equiv N stretching mode in SCN^- are sensitive to such interactions [29]. The observed shift in peaks position and intensity reveals the complexation was occurred between polymer CA and salt NH_4SCN .

The possible interaction between polymer CA and salt NH_4SCN was shown in Fig. 3. Generally, the proton conduction could occur either by the lone pair migration mechanism [30, 31] or vehicular mechanism (proton carried migration mechanism). In this case, lone proton migration (H^+) mechanism was more reasonable. In NH_4SCN , the hydrogen bonding occurs with N–H bond in the tetrahedral ion. The NH_4^+ pointing directly towards the thiocyanate ion (SCN^-) and form N–H... SCN hydrogen bond. In NH_4 ion, three hydrogen atoms were bounded strongly with nitrogen in which fourth hydrogen ion was weakly bound to it. The weakly bound H^+ of NH_4^+ can easily be dissociated under the influence of electric field and H^+ ions hop through the coordinating site (C=O) of the host polymer CA. Hence, the FTIR spectra confirm the interaction between polymer CA and salt NH_4SCN .

The shift in frequency of the C=O group in polymer CA is correlated with force constant. The force constant values can be calculated from the expression [32]

$$v = \frac{1}{2\pi c} \sqrt{k/\mu} \quad (1)$$

where, v is the wavenumber (cm^{-1}), c is the velocity of light ($3 \times 10^{10}\text{ cm s}^{-1}$), k is the force constant (Ncm^{-1}) and $\mu = M_1M_2/(M_1 + M_2)$. Here, μ is the reduced mass and M_1, M_2 are the atomic weight of two atoms

Table 1 FTIR assignments of all prepared polymer electrolytes

| PURE CA (cm ⁻¹) | 90CA:10 NH ₄ SCN (cm ⁻¹) | 80CA:20 NH ₄ SCN (cm ⁻¹) | 70CA:30 NH ₄ SCN (cm ⁻¹) | 60CA:40 NH ₄ SCN (cm ⁻¹) | 50CA: 50NH ₄ SCN (cm ⁻¹) | Assignments |
|--------------------------------|--|--|--|--|---|---------------------------------|
| – | – | 2055 | 2049 | 2056 | 2053 | C≡N stretching |
| 1736 | 1736 | 1736 | 1735 | 1733 | 1733 | C=O symmetric stretching |
| 1436 | 1436 | 1432 | 1429 | 1432 | 1432 | CH ₃ bending |
| 1371 | 1372 | 1371 | 1373 | 1371 | 1370 | C–H bending |
| 1219 | 1222 | 1222 | 1221 | 1222 | 1225 | C–O stretching |
| 1030 | 1030 | 1030 | 1031 | 1033 | 1028 | C–O–C stretching of pyrose ring |
| 901 | 908 | 905 | 901 | 905 | 908 | CH ₂ rocking |

respectively. The force constant values were calculated for pure CA and CA doped with different concentration of salt NH₄SCN. It was found that force constant value decreases from 1215 to 1205 N cm⁻¹ for C=O stretching. The decrease in force constant is due to the interaction of H⁺ ion in salt (NH₄SCN) and oxygen atom in polymer (CA), which weakens the C=O bond by the removal of electron density from it. Similar study was done for the polymer electrolyte [33]. These results confirm the complexation of polymer matrix.

3.3 Differential scanning calorimetry

DSC analysis was carried out to predict the glass transition temperature (T_g) of polymer electrolyte. The change in T_g of CA due to the addition of salt (NH₄SCN) was shown in Fig. 4a, b. The T_g of pure CA was obtained as 72.4 °C. The

T_g value was obtained as 81.5, 113.7 and 111.6 °C correspond to the 60CA:40NH₄SCN, 50CA:50NH₄SCN and 40CA:60NH₄SCN. The DSC curve (Fig. 4a, b) indicates that the T_g value of CA increases corresponding to the

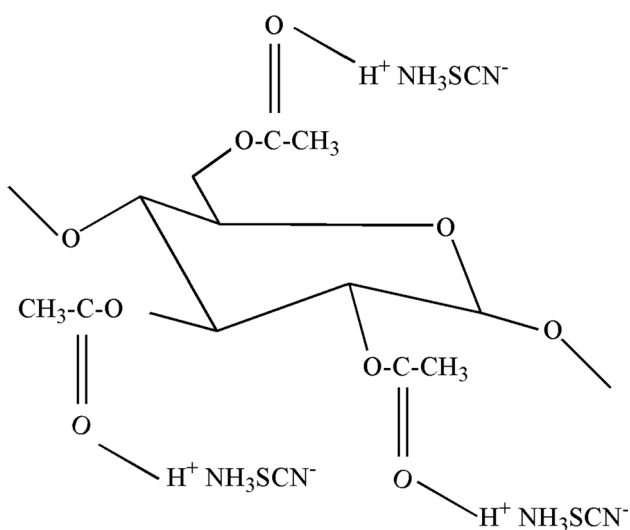


Fig. 3 Possible interaction between the polymer CA and the dopant NH₄SCN

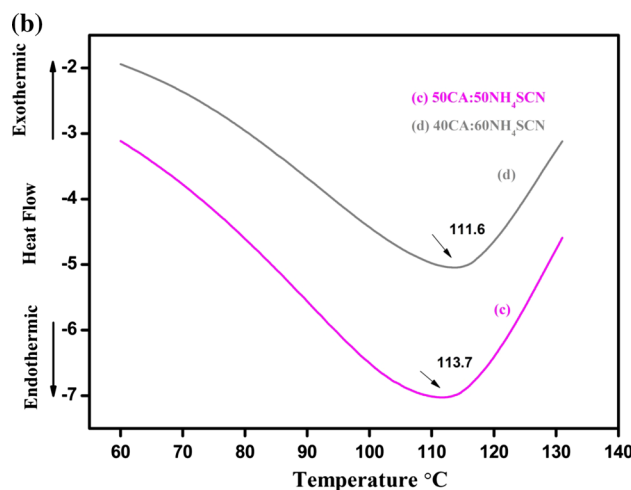
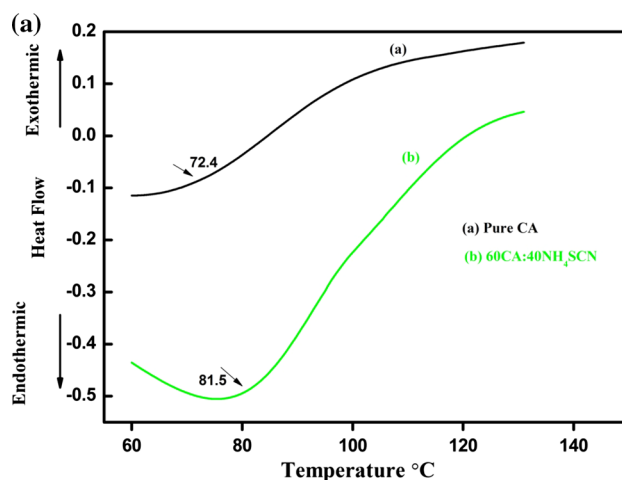


Fig. 4 a DSC thermo grams of PURE CA and 60CA:40NH₄SCN. b DSC thermo grams of 50CA:50NH₄SCN and 40CA:60NH₄SCN

increase in the concentration of NH_4SCN . In general, the decrease in glass transition temperature increases the ionic conductivity. In the present investigation, the observed DSC results were contrary to this. This behavior has been interpreted as a consequence of a reduction in segmental motion caused by an increase in intermolecular and intermolecular coordinations between H^+ cations and the oxygen atoms in the polymer chain [34]. The results are similar to those obtained by other authors with poly(epichlorohydrin-coethylene oxide) [P(EH/EO)s] and a structurally related polymer hosts [35, 36].

3.4 Electrochemical impedance spectroscopy analysis

Impedance spectroscopy is a powerful diagnostic tool to investigate the ionic conductivity of polymer electrolytes. The ionic conductivity mainly depends on the conducting species and their mobility. Figure 5 shows the Cole–Cole plot (Z' vs. Z'') for CA doped with different concentrations of NH_4SCN polymer electrolyte at room temperature (303 K). Generally, the impedance plot consists of a distorted semicircle in the high frequency region followed by an inclined spike in the low frequency region. The high frequency semicircle is due to the parallel combination of bulk resistance (due to migration of ions) and bulk capacitance (due to immobile polymer chain). The low frequency spike represented by a constant phase element is due to the formation of double layer capacitance at the electrode–electrolyte interface [37].

In the present investigation, the CA: NH_4SCN polymer electrolytes have only inclined spike and the semicircle was not observed, which indicates that the CA: NH_4SCN polymer

electrolyte have resistive component only and the capacitive nature of electrolyte were vanished, which is due to motion of charge carrier in the polymer electrolyte exists. The equivalent circuit was shown in Fig. 5. Electrochemical impedance spectroscopy (EIS) parameters were obtained from Cole to Cole plot by using EQ software program developed by Boukmap [38, 39], which were listed in Table 2. In Table 2, the resistance value of pure CA was obtained as $61.2 \times 10^3 \Omega$, whereas for 10–50 mol% of NH_4SCN doped with CA polymer electrolyte the value of resistance was decreased from 924 to 8.6 Ω . The constant phase element (CPE) value for pure CA was obtained as $2.66 \times 10^{-4} \mu\text{F}$. The NH_4SCN doped with CA polymer electrolyte have CPE values in the range of 3.37–2.75 μF . The highest conductivity polymer electrolyte 50CA:50 NH_4SCN has $R_b = 8.6 \Omega$ and $\text{CPE} = 2.75 \mu\text{F}$.

The ionic conductivity (σ) of the polymer electrolytes is calculated using the equation

$$\sigma = \frac{L}{A \times R_b} \text{ S cm}^{-1} \quad (2)$$

where L is the thickness, R_b is the bulk resistance and A is the contact area of the electrolyte film. The calculated ionic conductivity for different concentrations of CA: NH_4SCN polymer electrolytes were listed in Table 3 for various temperature. The Table 3 indicates that among the various concentrations of CA: NH_4SCN polymer electrolyte the 50CA:50 NH_4SCN polymer electrolyte has highest ionic conductivity ($3.31 \times 10^{-3} \text{ S cm}^{-1}$) at room temperature, which also has greater conductivity than that of pure CA ($1.285 \times 10^{-7} \text{ S cm}^{-1}$). The higher ionic conductivity of 50CA:50 NH_4SCN may be arises due to the transition from semicrystalline phase to an amorphous phase of polymer complex and increase in charge carrier concentration [40]. The Table 3 also indicates that the ionic conductivity is increases with respect to the increase in salt concentration. The reason for the conductivity enhancement was the polymer-salt interaction, especially the interaction of NH_4SCN with side chain of the polymer CA, but not much with the backbone of the main chain, which has little effect on the mobility of H^+ ions at ambient temperature [41].

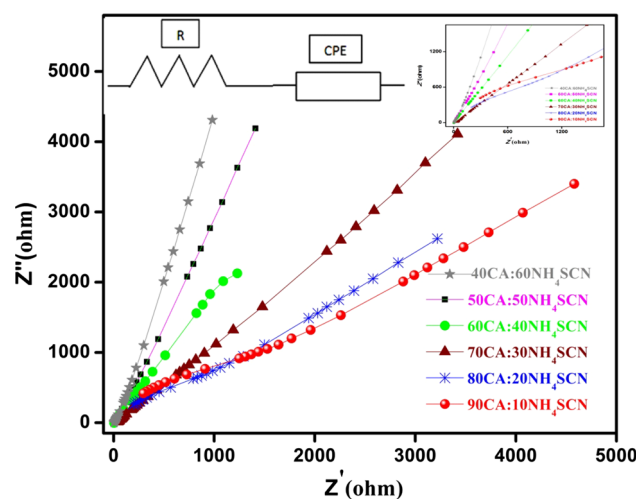


Fig. 5 Cole-Cole plot for pure CA, 90CA:10 NH_4SCN , 80CA:20 NH_4SCN , 70 CA:30 NH_4SCN , 60CA:40 NH_4SCN , 50CA:50 NH_4SCN , and the equivalent circuit

Table 2 EIS parameters for all polymer electrolytes

| Polymer composition (mol%) | R, Ω | CPE, μF |
|----------------------------------|--------------------|-----------------------|
| PURE CA | 61.2×10^3 | 2.66×10^{-4} |
| 90 CA:10 NH_4SCN | 924 | 3.37 |
| 80 CA:20 NH_4SCN | 236.7 | 4.64 |
| 70 CA:30 NH_4SCN | 30.94 | 9.34 |
| 60 CA:40 NH_4SCN | 8.7 | 6.92 |
| 50 CA:50 NH_4SCN | 8.6 | 2.75 |

Table 3 Ionic conductivity data and activation energy values for CA:NH₄SCN polymer electrolyte for different temperature

| Polymer composition (mol%) | $\sigma_{303\text{ k}}$ | $\sigma_{313\text{ k}}$ | $\sigma_{323\text{ k}}$ | $\sigma_{333\text{ k}}$ | $\sigma_{343\text{ k}}$ | Activation energy E_a (ev) at room temperature | Regression value |
|----------------------------|-------------------------|-------------------------|-------------------------|-------------------------|-------------------------|--|------------------|
| 90CA:10NH ₄ SCN | 8.42×10^{-6} | 2.47×10^{-5} | 2.68×10^{-5} | 7.86×10^{-5} | 1.72×10^{-4} | 0.633 | 0.911 |
| 80CA:20NH ₄ SCN | 3.17×10^{-5} | 1.52×10^{-5} | 2.87×10^{-5} | 6.38×10^{-5} | 1.81×10^{-4} | 0.622 | 0.930 |
| 70CA:30NH ₄ SCN | 1.6×10^{-4} | 2.3×10^{-4} | 3.05×10^{-4} | 4.76×10^{-4} | 7.3×10^{-4} | 0.337 | 0.982 |
| 60CA:40NH ₄ SCN | 2.45×10^{-3} | 2.82×10^{-3} | 4.99×10^{-3} | 6.86×10^{-3} | 7.34×10^{-3} | 0.275 | 0.923 |
| 50CA:50NH ₄ SCN | 3.31×10^{-3} | 5.16×10^{-3} | 6.22×10^{-3} | 7.16×10^{-3} | 8.01×10^{-3} | 0.145 | 0.990 |

3.5 Conduction spectra analysis

In general, the conductance spectra can be divided into three regions, which are low frequency dispersion region, frequency independent plateau region and high frequency region. The low frequency dispersion region represents the space charge polarization at the blocking electrodes. The frequency independent plateau region on the log σ (y-axis) gives dc conductivity (σ_{dc}) of polymer complex and the high frequency region corresponds to the bulk relaxation phenomenon, which is due to the coulombic interaction of charge carrier and disorder within the structure [42].

The variation of frequency dependent ac conductivity spectra for different concentration of NH₄SCN doped with CA was shown in Fig. 6. The σ_{dc} values for highest conductivity sample (50CA:50NH₄SCN) has been calculated by extrapolating the plateau region to log σ axis. The conductivity values obtained from the conduction spectra coincide with the bulk conductivity values obtained from Cole to Cole plot. The frequency dependent high frequency dispersion region for polymer electrolytes at room temperature were analyzed using Jonscher’s power law relation [43]

$$\sigma(\omega) = \sigma_{dc} + A\omega^\alpha \tag{3}$$

where σ_{dc} is the dc conductivity, A and α are temperature dependent parameters. By fitting experimental data into the Jonscher’s equation the value of α has been evaluated. The α values were calculated for the 80CA:20NH₄SCN and 90CA:10NH₄SCN polymer electrolyte from the high frequency dispersion region. The calculated α values of 0.60 and 0.63 correspond to the 80CA:20NH₄SCN and 90CA:10NH₄SCN at room temperature. The 80CA:20NH₄SCN and 90CA:10NH₄SCN polymer electrolytes have less than one α values, which indicate that the presence of free site for the next hop and the backward motion is slower due to the coulombic interaction between the ions [44].

3.6 Temperature dependent conductivity

The temperature dependent ionic conductivity nature for the complex CA:NH₄SCN polymer electrolyte was carried out over the temperature range 303–343 K. Figure 7a

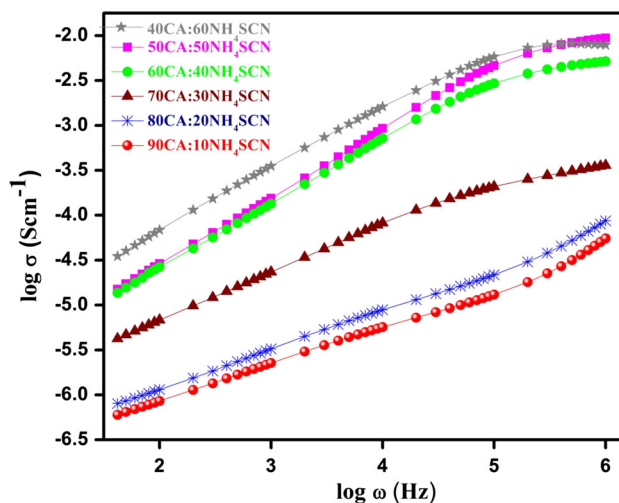


Fig. 6 Conduction plot for pure CA, 90CA:10NH₄SCN, 80CA:20NH₄SCN, 70 CA:30NH₄SCN, 60CA:40NH₄SCN, and 50CA:50NH₄SCN

shows the conductivity plot drawn between log (σ) and $1000/T$, which indicates that the conductivity increases with increasing temperature for all compositions. The membrane does not release any heat. The linear variation of ionic conductivity with inverse of absolute temperature follows Arrhenius relation

$$\sigma = (\sigma_0/T) \exp(-E_a/KT) \tag{4}$$

where, σ_0 is the pre-exponential factor, E_a is the activation energy and K is the Boltzmann constant. Activation energy (E_a) values were calculated for all prepared polymer electrolytes by the linear fitting of Arrhenius plots. Figure 7b, relates the conductivity and activation energy values of all composition of CA:NH₄SCN polymer electrolyte, which were listed in Table 3. The Table 3 indicates that the activation energy value of the polymer electrolyte decreases with increase in NH₄SCN concentration, which may due to the increase of amorphous nature of the polymer electrolyte.

3.7 Dielectric spectra analysis

In the present investigation, the dielectric properties of CA:NH₄SCN polymer electrolytes were characterized by

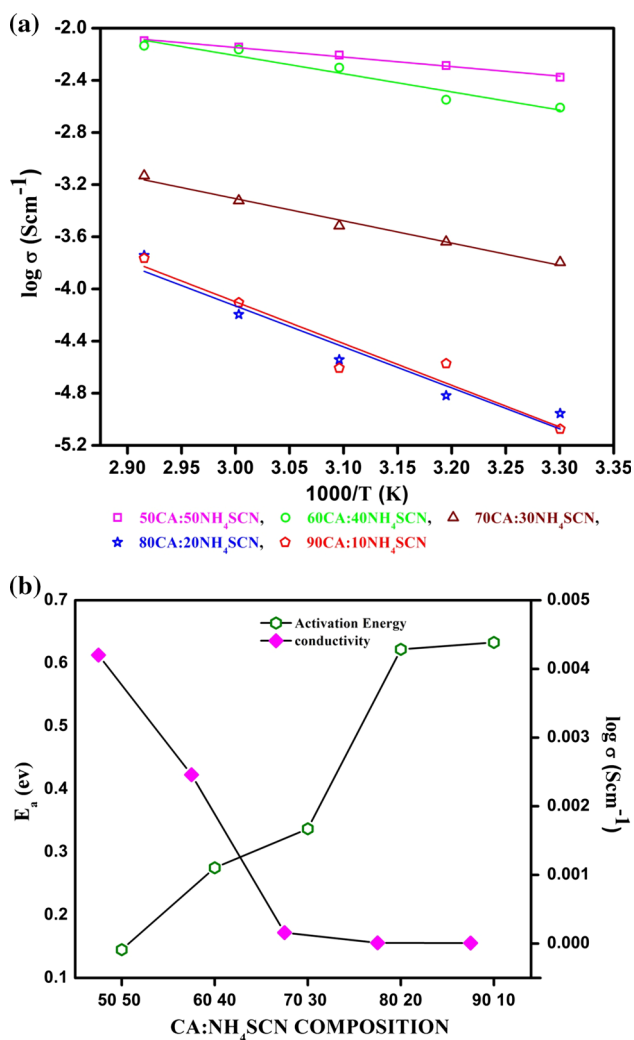


Fig. 7 **a** Temperature dependence ionic conductivity of 90CA:10NH₄SCN, 80CA:20NH₄SCN, 70 CA:30 NH₄SCN, 60CA:40NH₄SCN, and 50CA:50NH₄SCN. **b** Conductivity and activation energy of 90CA:10NH₄SCN, 80CA:20NH₄SCN, 70 CA:30 NH₄SCN, 60CA:40 NH₄SCN, and 50CA:50NH₄SCN

frequency dependent parameters, which bring about important insights into the ionic transport phenomenon [45]. The measured dielectric data describe the real and imaginary parts of the complex permittivity (ϵ^*), which is defined by the relation

$$\epsilon^* = \epsilon' - i\epsilon'' = \epsilon' - i(\sigma'/\omega\epsilon_0) \quad (5)$$

where, ϵ' is the real part of the dielectric constant, ϵ'' is the imaginary part of the dielectric constant of the material, σ' is the real part of conductivity, ω is the angular frequency and ϵ_0 is the permittivity of free space. Figure 8a, b represent the frequency dependence of $\epsilon'(\omega)$ and $\epsilon''(\omega)$ at room temperature. Figure 8a, b indicates that the values of both ϵ' and ϵ'' sharply increases towards low frequencies for all compositions of the polymer electrolyte, which is due to

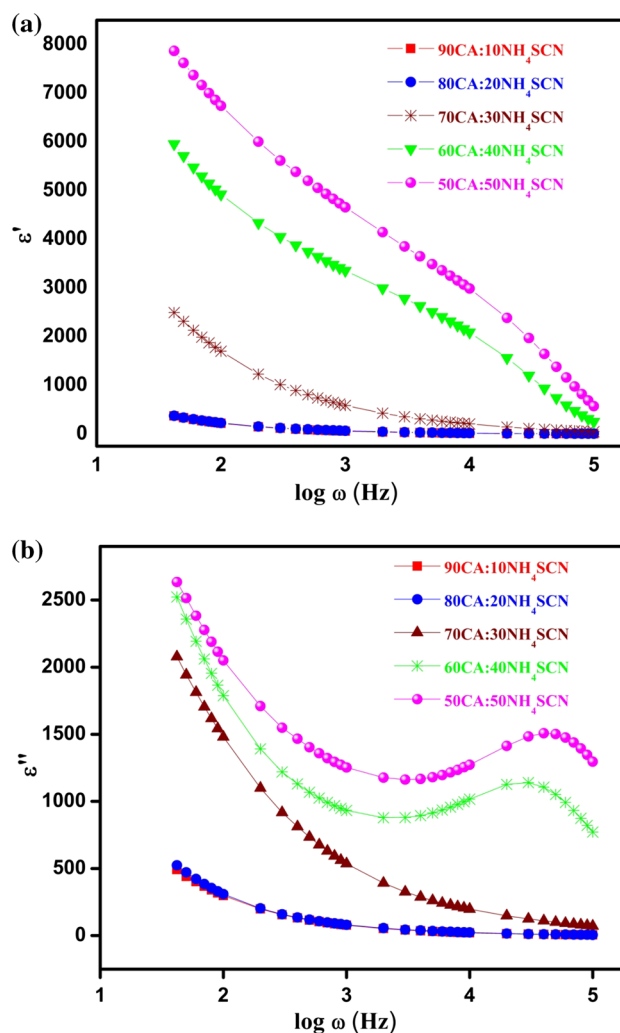


Fig. 8 **a** Frequency dependence of $\epsilon'(\omega)$ of 90CA:10NH₄SCN, 80CA:20NH₄SCN, 70 CA:30 NH₄SCN, 60CA:40NH₄SCN, and 50CA:50NH₄SCN. **b** Frequency dependence of $\epsilon''(\omega)$ of 90CA:10NH₄SCN, 80CA:20NH₄SCN, 70 CA:30 NH₄SCN, 60CA:40NH₄SCN, and 50CA:50NH₄SCN

the presence of space charge effect [46]. This type of behavior is known as the non-Debye nature, where the space charge region with respect to the frequency is explained in terms of diffusion [47]. The increase in dielectric constant denotes increase in the charge concentration within the polymer electrolytes. A significant high dielectric constant was obtained for the high conductivity 50CA:50NH₄SCN polymer electrolyte. Figure 8a, b describe that when the frequency increases, the value of ϵ' and ϵ'' decrease and reaches saturation, which is due to the periodic reversal of the applied electric field takes place so rapidly that the mobile ion will not be able to orient themselves in the field direction resulting it to saturate or decrease the dielectric constant [48].

3.8 Modulus spectra analysis

In general, the ion transport process of ionic conductors is studied in terms of electrical modulus spectrum. Figure 9a, b represent the frequency dependence of $M'(\omega)$ and $M''(\omega)$ at room temperature. Both M' and M'' are observed to increase in the high frequency end. At low frequencies, the value of $M'(\omega)$ and $M''(\omega)$ decreases, which is due to the electrode polarization phenomenon and makes a negligible contribution. For all CA:NH₄SCN complex the modulus value gradually increases with increase of frequencies, which is due to bulk effect. The plot that shows long tails at low frequencies are due to their large capacitance values associated with electrodes [49].

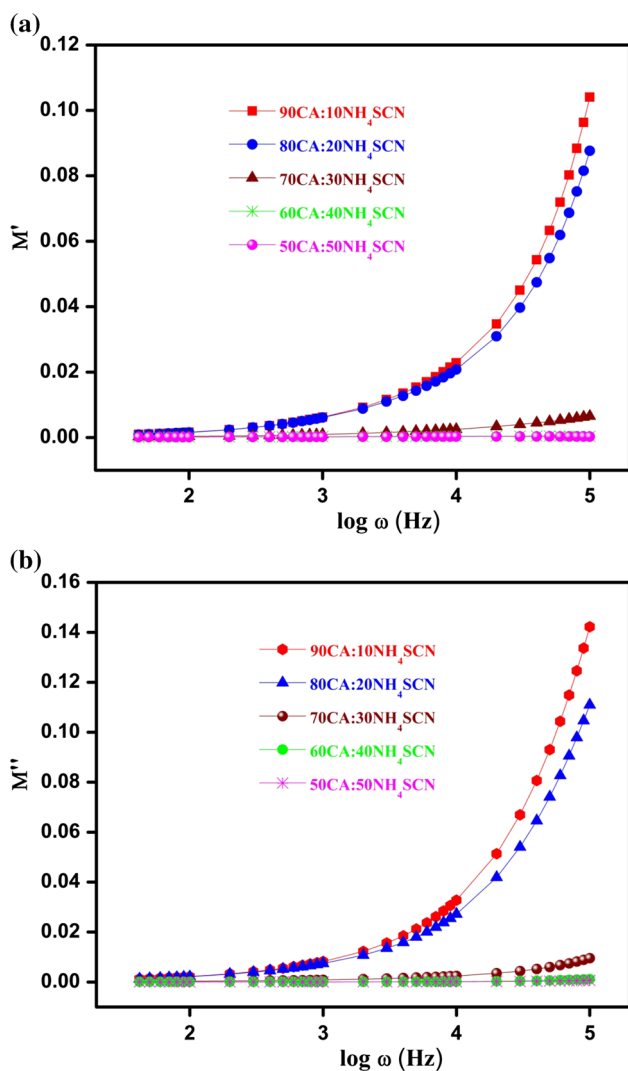


Fig. 9 a Frequency dependence of $M'(\omega)$ of 90CA:10NH₄SCN, 80CA:20NH₄SCN, 70 CA:30 NH₄SCN, 60CA:40NH₄SCN, and 50CA:50NH₄SCN. b Frequency dependence of $M''(\omega)$ of 90CA:10NH₄SCN, 80CA:20NH₄SCN, 70 CA:30 NH₄SCN, 60CA:40NH₄SCN, and 50CA:50NH₄SCN

3.9 Transference number measurement

The ionic transference number is the most important parameter to identify the specific type of charged species (ions/electron) present in polymer electrolytes.

The transference numbers are calculated using the equations [50]

$$t_{ion} = (I_i - I_f) / I_i \tag{6}$$

$$t_{elec} = I_f / I_i \tag{7}$$

where, I_i is the initial current and I_f is the final current.

To determine the total charge transport of the polymer electrolyte film, cell with a configuration, stainless steel/50CA:50NH₄SCN/stainless steel was prepared and polarized by applying a constant dc potential of 1.08 V. The polarization current versus time for 50CA:50NH₄SCN polymer electrolyte film at 303 K was shown in Fig. 10. Initially, the polarization current decreases with time, which happens when the migration of ions due to the applied field balanced by diffusion and hence leads to the cell polarization [51].

The value of ionic transference (t_{ion}) number for the highest conducting polymer electrolyte film 50CA:50NH₄SCN was found to be ~0.99. This suggests that the charge transport in this polymer electrolyte was primarily due to ions, which are close to unity and only a negligible contribution comes from the electron. The diffusion coefficients of cations and anions of 60CA:40NH₄SCN, 50CA:50NH₄SCN, 40CA:60NH₄SCN were calculated using the following equations [52], which were listed in Table 4.

$$D = D_+ + D_- = \frac{KT\sigma}{ne^2} \tag{8}$$

$$t_+ = \frac{D_+}{D_+ + D_-} \tag{9}$$

The ionic mobility of cations and anions of all the samples is calculated using the following equations.

$$\mu = \mu_+ + \mu_- = \frac{\sigma}{ne} \tag{10}$$

$$t_+ = \frac{\mu_+}{\mu_+ + \mu_-} \tag{11}$$

where, e is the charge of the electron, k Boltzmann constant, T absolute temperature, n is the number of charge carriers stoichiometrically related to the salt composition, μ_+ and μ_- is the ionic mobility of cation and anion respectively and D_+ and D_- is the diffusion coefficients of cation and anion respectively. The Table 4 indicates that the cation mobility of μ_+ has greater value than the ionic mobility of anions μ_- . When μ_+ decreases, the conductivity also decreases and vice versa. The same behavior also can be detected for D_+ . Highest mobility

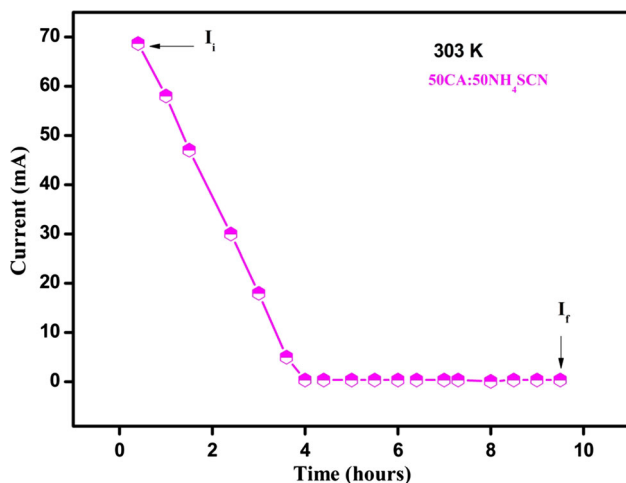


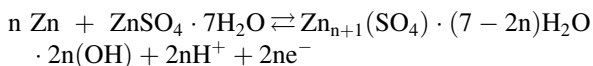
Fig. 10 Polarization current versus time plot for 50CA:50NH₄SCN

$8.13 \times 10^{-6} \text{ cm}^2 \text{ V}^{-1} \text{ s}^{-1}$ was observed for 50CA:50NH₄SCN.

3.10 Fabrication and characterization of primary proton battery

Proton battery was constructed using the highest conducting sample 50CA: 50NH₄SCN. Anode was prepared using Zn (metal powder), ZnSO₄·7H₂O and graphite powder in the desired proportions (3:1:1) and made to form thin pellet. Similarly the cathode material was prepared using PbO₂, V₂O₅, graphite and polymer electrolyte in the desired ratio of (8:2:1:0.5) and finally made into a thin pellet. The polymer electrolyte was sandwiched between anode and cathode pellets. The battery configuration was shown in Fig. 11. The open circuit voltage (OCV) of the cell was allowed to stabilize for certain duration to attain a constant voltage. The stabilized voltage of 1.3 V was monitored with respect to time and presented in Fig. 12a.

The anode reaction is given as follows:



The cathode reaction is given as follows:

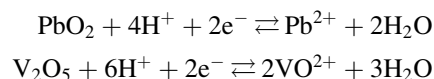


Table 4 Ionic mobility and diffusion coefficient of cations and anions

| Polymer composition (mol%) | $n \text{ (cm}^{-3}\text{)}$ | t_{ion} | $D_+ \text{ (cm}^2 \text{ s}^{-1}\text{)}$ | $D_- \text{ (cm}^2 \text{ s}^{-1}\text{)}$ | $\mu_+ \text{ (cm}^2 \text{ V}^{-1} \text{ s}^{-1}\text{)}$ | $\mu_- \text{ (cm}^2 \text{ V}^{-1} \text{ s}^{-1}\text{)}$ |
|-----------------------------|------------------------------|------------------|--|--|---|---|
| 60CA:40 NH ₄ SCN | 4.22×10^{21} | 0.98 | 2.45×10^{-8} | 5.03×10^{-10} | 9.39×10^{-7} | 1.91×10^{-8} |
| 50CA:50 NH ₄ SCN | 3.19×10^{21} | 0.99 | 2.12×10^{-7} | 2.15×10^{-9} | 8.13×10^{-6} | 8.27×10^{-8} |
| 40CA:60 NH ₄ SCN | 2.36×10^{21} | 0.99 | 1.66×10^{-7} | 1.69×10^{-9} | 6.39×10^{-6} | 6.46×10^{-8} |

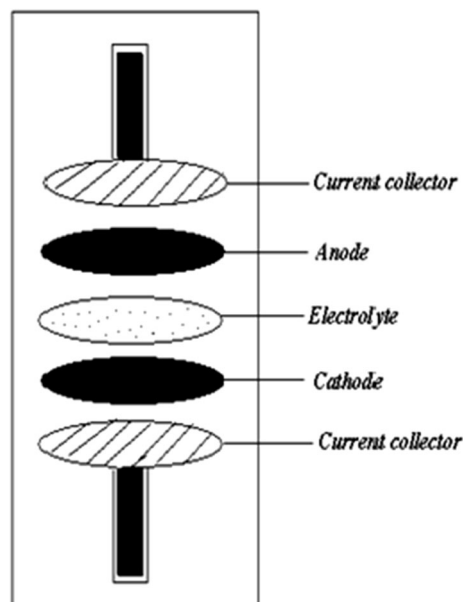


Fig. 11 Battery holder

The stabilized voltage of 1.32 V observed in the cell was discharged through 1 M Ω load resistance at room temperature. Discharge behavior of the cell with time was shown in Fig. 12b, which indicates that the cell potential decreases during discharge. The initial sharp decreasing in voltage may be due to polarization [53] and it remains constant for a particular duration after which there was a decline in voltage. The region in which the voltage remains constant is called as the plateau region. The OCV and discharge time for plateau region and other cell parameters for this cell were listed in Table 5.

4 Conclusions

In this work, the new biodegradable and high proton conducting polymer electrolyte based on CA:NH₄SCN was prepared by the method of solution casting. XRD analysis suggested an increase in the amorphous nature with increase in NH₄SCN salt concentrations in the polymer matrix. FTIR study confirms the complexation of the polymer with the dopant salt. The temperature dependence ionic conductivity follows the Arrhenius relation. The

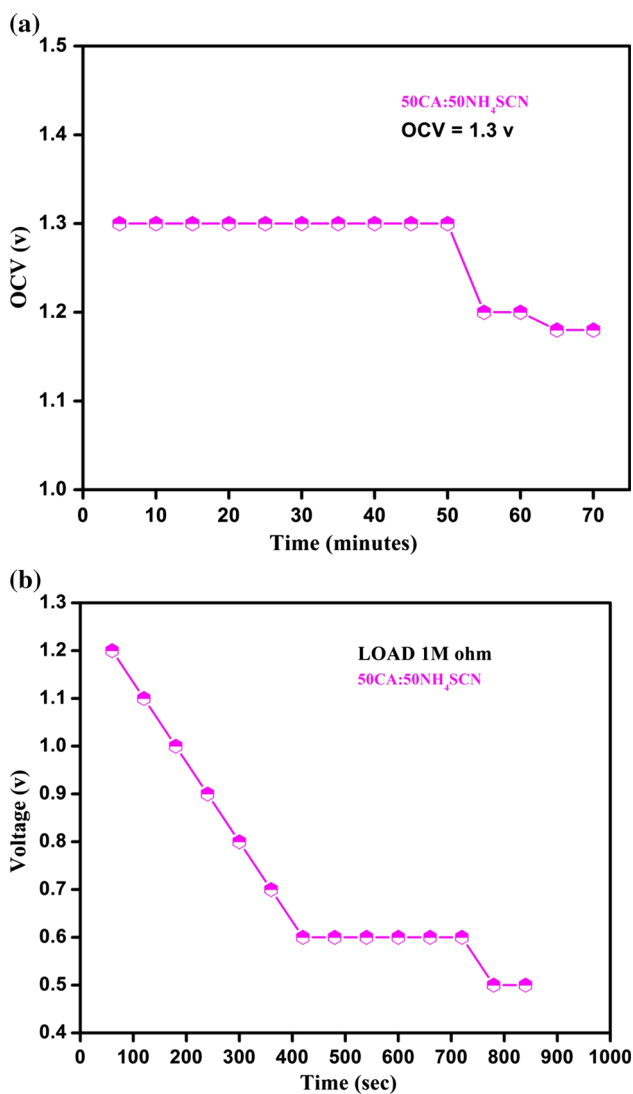


Fig. 12 **a** Open circuit voltage as a function of time for 50CA:50NH₄SCN polymer electrolyte. **b** Discharge curves for cell using 1 MΩ for 50CA:50NH₄SCN polymer electrolyte

Table 5 Important cell parameters

| | |
|---|-------|
| Cell area (cm ²) | 0.895 |
| Cell weight (g) | 1.284 |
| Effective cell diameter (cm) | 1 |
| Cell thickness (cm) | 0.288 |
| Open circuit voltage (OCV) (V) | 1.3 |
| Discharge time for plateau region (min) | 30 |

highest conductivity $3.31 \times 10^{-3} \text{ S cm}^{-1}$ was achieved for the 50CA:50NH₄SCN polymer electrolyte with lowest activation energy 0.145 eV. Transference number data show that the conductivity was mainly arises due to ions rather than electrons. Thus, the optimized polymer

electrolyte 50CA:50NH₄SCN with high conductivity was applied for primary proton battery and their main parameters were reported. As a conclusion, the utilization of biopolymer electrolyte, such as CA:NH₄SCN with novel, challenging, cheap and environmentally benign may have not only suits for its superior ion conducting properties, but also implied for energy storage devices such as fuel cell and batteries.

References

1. A. Karmakar, A. Ghosh, Dielectric permittivity and electric modulus of polyethyleneoxide (PEO)-LiClO₄ composite electrolyte. *Curr. Appl. Phys.* **12**(2), 539–543 (2012)
2. W.H. Meyer, Polymer electrolytes for lithium-ion batteries. *Adv. Mater.* **10**(6), 439–448 (1998)
3. A.S. Ahmad Khair, A.K. Arof, Conductivity studies of starch-based polymer electrolytes. *Ionics* **16**, 123–129 (2010)
4. K. Pradeep, Varshney, Shikha Gupta, natural polymer-based electrolytes for electrochemical devices: a review. *Ionics* **17**, 479–483 (2011)
5. L. Ponez, F.C. Sentanin, S.R. Majid, A.K. Arof, A. Pawlicka, Ion-conducting electrolytes based on gelatin and containing LiI/2 for electrochromic devices. *Mol. Cryst. Liq. Cryst.* **554**, 239–251 (2012)
6. S.B. Aziz, Z.H.Z. Abidin, A.K. Arof, Effect of silver nanoparticles on the dc conductivity in Chitosan silvertriflate polymer electrolyte. *Phys. B* **405**, 4429–4433 (2010)
7. N.A. Nik Aziz, N.K. Idris, M.I.N. Isa, Proton conducting polymer electrolyte methylcellulose doped ammonium fluoride: conductivity and ionic transport study. *Int. J. Phys. Sci.* **5**(6), 748–752 (2010)
8. A. Daniel Cerqueira, J.M. Artur Valente, R. Guimes Filho, D. Hugh Burrows, Synthesis and properties of polyaniline-cellulose acetate blends: the use of sugarcane bagasse waste and the effect of the substitution degree. *Carbohydr. Polym.* **78**, 402–408 (2009)
9. S. Ramesh, R. Shanthi, Ezra Morris, characterization of conducting cellulose acetate based polymer electrolytes doped with “green” ionic mixture. *Carbohydr. Polym.* **9**, 14–21 (2013)
10. S. Ramesh, R. Shanthi, Ezra Morris, plactizing effect of 1-allyl-3-methylimidazolium chloride in cellulose acetate based polymer electrolytes. *Carbohydr. Polym.* **87**, 2624–2629 (2012)
11. N.A. Johari, T.I.T. Kudin, A.M.M. Ali, T. Winie, M.Z.A. Yahya, Studies on cellulose acetate-based gel polymer electrolytes for proton batteries. *Mater. Res. Innov.* **13**(3), 232–234 (2009)
12. N.A. Johari, T.I.T. Kudin, A.M.M. Ali, M.Z.A. Yahya, Electrochemical studies of composite cellulose acetate-based polymer gel electrolytes for proton. *Proc. Natl. Acad. Sci. Sect. A Phys. Sci.* **82**(1), 49–52 (2009)
13. G.M. Wu, S.J. Lin, C.C. Yang, in *Fuel Cell Research Trends*, ed. by L.O. Vasquez (Nova Science Publishers, Inc., Newyork, 2007), p. 448
14. S.Z.Z. Abidin, A.M.M. Ali, O.H. Hassan, M.Z.A. Yahya, Electrochemical studies on cellulose acetate-LiBOB polymer gel electrolytes. *Int. J. Electrochem. Sci.* **8**, 7320–7326 (2013)
15. M. Selvakumar, D. Krishna Bhat, *LiClO₄ Doped Cellulose Acetate as Biodegradable Polymer Electrolyte for Supercapacitors* (Wiley, Hoboken, 2008). doi:10.1002/app.28671
16. S. Chandra, S.A. Hashmi, G. Prasad, Studies on ammonium perchlorate doped polyethyleneoxide polymer electrolyte. *Solid State Ion.* **40–41**, 651–654 (1990)

17. M. Kumar, S. Sekhon, Role of plasticizer's dielectric constant on conductivity modification of PEO-NH₄F polymer electrolytes. *Eur. Polym. J.* **38**, 1297–1304 (2002)
18. F.M. Gray, *Solid Polymer Electrolytes* (VCH Publishers Inc, New York, 1991)
19. S.A. Hashmi, A. Kumar, K.K. Maurya, S. Chandra, Proton-conducting polymer electrolyte. I. The polyethylene oxide + NH₄ClO₄ system. *J. Phys. D Appl. Phys.* **23**(10), 1307 (1993)
20. N.A. Aziza, S.R. Majida, R. Yahyaa, A.K. Arof, Conductivity, structure, and thermal properties of chitosan-based polymer electrolytes with nanofillers. Wiley Online Lib. (2009). doi:10.1002/pat.1619
21. M.F. Shukur, Y.M. Yusof, S.M.M. Zawawi, H.A. Illias, M.F.Z. Kadir, Conductivity and transport studies of plasticized Chitosan-based proton conducting biopolymer electrolytes. *Phys. Scr.* **57**, 014050 (2013)
22. M.P. Aji, Masturi, S. Bijaksana, Khairurrijal, M. Abdullah, A general formula for ion concentration dependent electrical conductivities in polymer electrolytes. *Am. J. Appl. Sci.* **9**(6), 946–954 (2012)
23. R. Baskaran, S. Selvasekarapandian, N. Kuwata, J. Kawamura, T. Hattori, Conductivity and thermal studies of blend polymer electrolytes based on PVAc-PMMA. *Solid State Ion.* **177**(26), 2679–2682 (2006)
24. R.M. Hodge, G.H. Edward, G.P. Simon, Water absorption and states of water in semicrystalline poly(vinyl alcohol) films. *Polymer* **37**, 1371–1376 (1996)
25. M.F.Z. Kadir, S.R. Majid, A.K. Arof, Plasticized chitosan-PVA blend polymer electrolyte based proton battery. *Electrochim. Acta* **55**, 1475–1482 (2010)
26. M. Ali, Influence of glycol additives on the structure and performance of cellulose acetate/zinc oxide blend electrolytes. *Desalination* **270**, 98–104 (2011)
27. G. Hirankumar, S. Selvasekarapandian, M.S. Bhuvaneswari, R. Baskaran, M. Vijayakumar, AC impedance studies on proton conducting polymer electrolyte complexes (PVA + CH₃COONH₄). *Ionics* **10**, 135–138 (2004)
28. M. Xu, E.M. Eyring, S. Petrucci, Molecular dynamics and infrared spectra of NaSCN dissolved in the solvent macrocycle 15-crown-5 and polyethylene oxide dimethyl ether-250. *J. Phys. Chem.* **99**(40), 14589–14596 (1995)
29. H. Zhang, X. Xuan, J. Wang, H. Wang, FT-IR investigation of ion association in PEO-MSCN (M = Na, K) polymer electrolytes. *Solid State Ion.* **164**, 73–79 (2003)
30. A. Pottier, *The Hydrogen Bond and Chemical Parameters Favoring Proton Mobility in Solid*, in *Proton Conductors: Solid, Electrolytes and Gel Materials and Devices* (Cambridge University Press, Cambridge, 1992)
31. T. Norby, *Solid State Ion.* **125**, 1–11 (1999)
32. B.H. Stuar, *Infrared Spectroscopy: Fundamentals and Applications* (Wiley, Colorado, 2004)
33. H. Nithya, Ph.D thesis entitled Characterization of polymer electrolyte poly(Epichlorohydrin-ethyleneoxide): LiClO₄ (2011)
34. C.A. Angell, K. Xu, S.S. Zhang, N. Videa, Variations on the salt-polymer electrolyte theme for flexible solid electrolytes. *Solid State Ion.* **86–88**, 17–28 (1996)
35. W.A. Gazotti, M.A.S. Spinacé, E.M. Giroto, M.A. De Paoli, Polymer electrolytes based on ethylene oxide-epichlorohydrin copolymers. *Solid State Ion.* **130**, 281–291 (2000)
36. G.G. Silva, N.H.T. Lemes, C.N. Polo da Fonseca, M.A. De Paoli, Solid state polymeric electrolytes based on poly (epichlorohydrin). *Solid State Ion.* **93**, 105–116 (1997)
37. J.R. Macdonald (ed.), *Impedance Spectroscopy* (Wiley, New York, 1987)
38. B.A. Boukamp, *Solid State Ion.* **20**, 301 (1986)
39. B.A. Boukamp, *Solid State Ion.* **18&19**, 136 (1986)
40. H. Nithya, S. Selvasekarapandian, P. ChristopherSelvin, D. ArunKumar, M. Hema, D. Prakash, Characterization of nanocomposite polymer electrolyte based on P(ECH-EO). *Phys. B* **406**, 3367–3373 (2011)
41. S.H. Kim, J.Y. Kim, H.S. Kim, H.N. Cho, Ionic conductivity of polymer electrolytes based on phosphate and polyether copolymers. *Solid State Ion.* **116**, 63–71 (1999)
42. C. Kim, G. Lee, K. Leo, K.S. Ryu, S.H. Chang, Polymer electrolytes prepared by polymerizing mixtures of polymerizable PEO-oligomers, copolymer of PVDC and poly(acrylonitrile), and lithium triflate. *Solid State Ion.* **123**, 251–257 (1999)
43. A.K. Jonscher, The universal dielectric response. *Nature* **267**, 673–679 (1977)
44. N. Rajeswari, C. Sanjeeviraja, J. Kawamura, S. Asath Bahadur, A study on polymer blend electrolyte based on PVA/PVP with proton salt. *Polym. Bull.* (2014). doi:10.1007/s00289-014-1111-8
45. J.R. Mac Callum, C.A. Vincent, low frequency dielectric properties of polyether electrolytes. *Elsevier Appl. Sci.* 43–60 (1989)
46. R. Mishra, K.J. Rao, Electrical conductivity studies of poly(ethyleneoxide)-poly(vinylalcohol) blends. *Solid State Ion.* **106**, 113–127 (1998)
47. R. Baskaran, S. Selvasekarapandian, N. Kuwata, J. Kawamura, T. Hattori, Ac impedance, DSC and FT-IR investigations on (x) PVAc-(1-x) PVdF blends with LiClO₄. *Mater. Chem. Phys.* **98**, 55–61 (2006)
48. K. Adachi, O. Urakawa, Dielectric study of concentration fluctuations in concentrated polymer solutions. *J. Non-Cryst. Solids* **307–310**, 667 (2002)
49. S. Ramesh, A.K. Arof, Ionic conductivity studies of plasticized poly(vinyl chloride) polymer electrolytes. *Mater. Sci. Eng. B* **85**, 11–15 (2001)
50. J.B. Wagner, C.J. Wagner, Electrical conductivity measurements on cuprous halides. *Chem. Rev.* **26**, 1597 (1957)
51. T. Winnie, A.K. Arof, Transport properties of hexanoyl chitosan based gel electrolyte. *Ionics* **12**, 149–152 (2006)
52. S. Chandra (ed.), *Superionic Solids—Principles and Applications*, North Holland, Amsterdam (1981)
53. K. Singh, R.U. Tiwari, V.K. Deshpande, Performance of a solid-state battery with a proton-conducting electrolyte. *J. Power Sour.* **1**, 65–71 (1993)